Lateral alloy segregation in thin heteroepitaxial films

J. M. Reich,[1] X. B. Niu,[2] Y.-J. Lee,[1] R. E. Caflisch,[1,2] and C. Ratsch[1,3]
[1]*Department of Mathematics, UCLA, Los Angeles, California 90095, USA*
[2]*Department of Material Sciences and Engineering, UCLA, Los Angeles, California 90095, USA*
[3]*Institute for Pure and Applied Mathematics, UCLA, Los Angeles, California 90095, USA*
(Received 6 June 2008; published 13 February 2009)

Alloy segregation is believed to be an important factor in the growth of the wetting layer and subsequent formation of islands during heteroepitaxy. We report simulated annealing results that determine the lowest-energy configuration of a strained system. Our results indicate that in addition to vertical segregation, there is also an energetic driving force for lateral segregation and formation of subsurface features before island formation. We believe that these subsurface features play a crucial role in the nucleation of islands.

DOI: 10.1103/PhysRevB.79.073405 PACS number(s): 68.55.−a, 68.65.Hb, 81.16.Dn

It is a well-established fact that for many heteroepitaxial systems growth proceeds in the Stranski-Krastanov growth mode, where islands form after the formation of a wetting layer.[1,2] But this wetting layer can be surprisingly thick, over 10 monolayers and more.[3–5] The driving forces that lead to the formation of this wetting layer and control its thickness are still not completely understood. Electronic effects can be ruled out when the thickness of the wetting layer is more than just a few atomic layers. Purely energetic effects are also implausible; unless there are some more subtle strain effects, there is no additional kinetic driving force for atoms to form islands in higher layers than there is in lower layers. So the question is: what drives the formation of islands after the deposition of a wetting layer?

Recent results suggest that intermixing might be a crucial factor in controlling the formation and thickness of the wetting layer. For example, for the system $In_xGa_{1-x}As$ on GaAs, kinetic Monte Carlo (KMC) simulations by Cullis and co-workers[5,6] suggest that some of the In atoms that are deposited can exchange with Ga atoms underneath, leading to a decreased In concentration in the top layer. When the next $In_xGa_{1-x}As$ layer is deposited, atoms exchange again. But some In atoms will only be able to exchange with an In atom underneath so that the In concentration cannot be reduced as effectively as before. As the deposited film gets thicker, the In concentration increases gradually, which implies an increase in the effective misfit. Eventually, the In concentration in the top layer (and thus the effective misfit) reaches a critical value, and the system prefers the formation of three-dimensional islands. This transition can occur at thicknesses that are many layers, and the critical thickness depends on the efficiency of the atoms to exchange and on the In concentration x. A similar mechanism has been proposed in a continuum model by Tu and Tersoff[7] for Ge_xSi_{1-x} on Si.

In previous work on this subject it has always been assumed that the vertical segregation is homogeneous, i.e., that the concentration of In increases with height, but that it is a spatial constant at any given height of the film. In this Brief Report we present results that suggest that in addition to vertical segregation there is also lateral segregation. This lateral segregation leads to spatial variations of the lattice constant on the surface and thus might ultimately be responsible for the lateral placement of islands on the surface. We show that purely energetic arguments do not predict a length scale, but we believe that kinetic limitations (or other additional physics) will introduce a length scale that defines a typical island separation.

Alloy segregation is a well-known phenomenon for many metals or semiconductors alloys in the bulk. But during epitaxy, the situation is typically different because separated phases have a higher strain energy than a mixed phase on a substrate. Our results suggest, however, that alloy segregation can indeed be stable during epitaxy because segregation can enhance the upward relaxation. Two types of lateral alloy segregation have been identified in previous research. Surface roughness provides a mechanism for alloy segregation that is kinetically driven (e.g., Priester and Grenet[8] for an atomistic model of heteroepitaxy). Spinodal decomposition is an energetically driven mechanism for segregation of alloys due to a nonmonotone thermodynamic driving force. Most studies of spinodal decomposition have been for bulk systems, but Huang and Desai,[9] for example, applied a spinodal decomposition analysis to determine the instability of a strained heteroepitaxial system. Our work presented here goes beyond these studies of instability at a continuum level to find the atomistic configuration that is energetically optimal. Alloying has also been found to be an important factor after islands have been formed[10–12] and in fact significantly affects the evolution of the size and shape of the islands. We note in particular the recent elegant KMC simulations in Refs. 13 and 14.

In our model we minimize the total energy of a simple 1+1 dimensional system with a cubic lattice that consists of two species. We believe that this simple model captures the essential physics and that different lattice structures will qualitatively behave similar. For simplicity, we label the two materials A and B, but they represent, for example, Si and Ge or GaAs and InAs. We assume that misfit and strain are the dominant effect and that the (unstrained) bond energy between any two atoms is the same (i.e., $E_{A\text{-}A}=E_{B\text{-}B}=E_{A\text{-}B}$). Since we only study the energetics of a flat film, before the formation of islands, this implies that the system with the lowest strain energy is also the system with the lowest total energy. Therefore, the problem is reduced to finding the atomic configuration that has the lowest elastic energy. Our model[15,16] assumes harmonic interactions that include nearest-neighbor interaction, next-nearest-neighbor (diago-

nal) interactions, and a bond-bending term, such that the energy can be written as

$$E = k(S_{xx}^2 + S_{yy}^2) + k_{\text{diag}}[(S_{xx} + 2S_{xy} + S_{yy})^2 + (S_{xx} - 2S_{xy} + S_{yy})^2] + k_{\text{bb}}S_{xy}^2. \quad (1)$$

The coefficients k, k_{diag}, and k_{bb} represent the spring constants for the nearest-neighbor, diagonal, and bond-bending springs, and the S_{ij} are the components of the strain tensor. We note that this expression can be rewritten such that the energy density can be interpreted as an atomistic as well as a continuum energy density.[16] We use periodic boundary conditions laterally and a fixed boundary condition at the bottom of the system.

Finding the lowest-energy configuration of a system within a high-dimensional parameter space is not an easy task. It is certainly not possible to calculate and compare the energy of all possible states of the system. In our study we have implemented a simulated annealing scheme. In general, the simulated annealing algorithm works as follows. We start with a random configuration of atoms of type A and B. We then generate at random a new configuration (typically by just swapping an A and a B atom). If the energy of the new configuration is lower, the swap is accepted. If it is higher, it is accepted with a probability that is related to $\exp(-\Delta E/k_B T_a)$, where ΔE is the energy difference between the initial and the final configuration, k_B is the Boltzmann constant, and T_a is the annealing temperature. The procedure is repeated many times. As T_a is lowered, the system converges, ideally to the true energetic minimum. We note that despite all our efforts to find efficient annealing schemes, we often found the true lowest-energy state by improving "by hand" upon the configuration found during the simulated annealing (more details below).

For all results presented in this paper we have chosen $k = 4 \times 10^{12}$ dyn/cm^2 (a typical value for semiconductors) and then varied k_{diag} and k_{bb} over several orders of magnitude. It turned out that variations in k_{bb} have only a weak effect, and we use (without a loss of generality) $k_{\text{bb}} = 2 \times 10^{12}$ dyn/cm^2 for all results shown below. The ratio $r = k/k_{\text{diag}}$ is then the most relevant parameter to characterize qualitatively different results for the lowest-energy configuration. The results shown in Figs. 1, 2, and 4 are for $r = 2$. We assume that the lattice constant of B atoms is 4% bigger than that of A atoms, but all results presented here are independent of the misfit. Furthermore, we assume that the equilibrium bond length between an A and a B atom is the average of the A-A and B-B bond lengths.

The configurations shown in Fig. 1(a)–1(e) represent typical annealing results for 40 and 64 B atoms, which are placed in an array of A atoms with a size of 20×20. We have carefully tested the importance of the system size and found that the results are essentially the same if we choose a bigger array of A atoms, keeping the same number of B atoms. For 40 B atoms, the configuration in Fig. 1(c) is lowest in energy, but the ones in Figs. 1(a) and 1(b) are only 0.068 and 0.143 eV higher in energy, respectively. Note for comparison that at a typical experimental growth temperature (twice the room temperature), $k_B T \sim 0.05$ eV. We have done many simulations for 40 B atoms and, in addition, have done many manual refinements and variations in these configurations. We have not found any configuration that is lower in energy than the one shown in Fig. 1(c) and therefore believe that this is the true energetic minimum. It can be described as a rectangular, essentially solid block of B atoms embedded in but at the top of the matrix of A atoms. The bottom row of B atoms is separated from the solid part by one row of A atoms. Configurations (a) and (b) are similar: in (a), only one atom is at a different position, while in configuration (b), we see two rows of B atoms at the bottom that are separated by rows of A atoms.

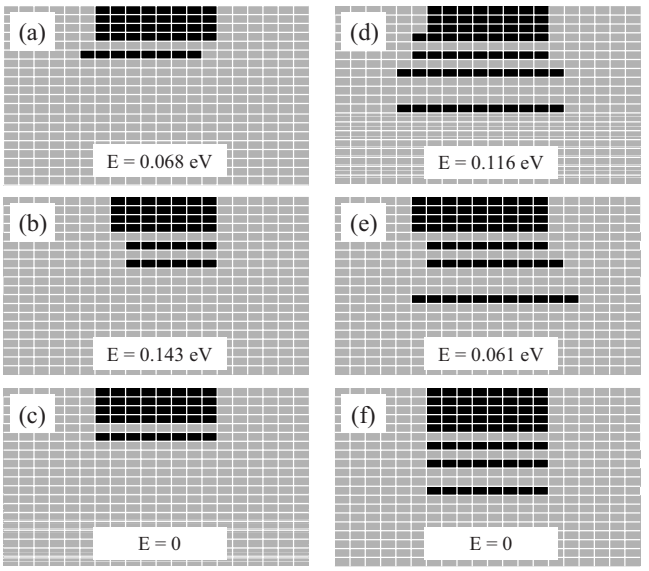

FIG. 1. Typical annealing results from independent annealing runs for [(a)–(c)] 40 B atoms (black) and [(d) and (e)] 64 B atoms in an array of A atoms (gray). We also show the lowest-energy configuration for 64 B atoms (f), which was obtained by manual tests, as described in the text. The energies are with respect to the lowest-energy configurations (c) and (f).

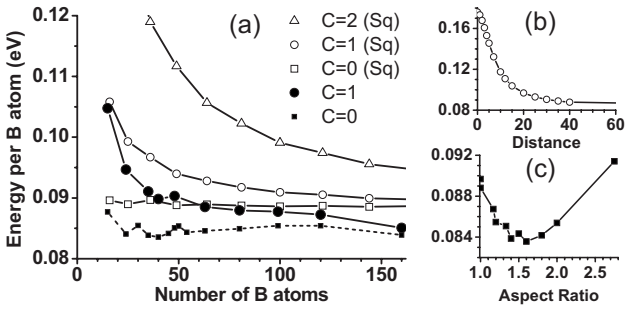

FIG. 2. (a) Elastic energy per B atom within a single solid feature for different numbers of B atoms within arrays of A atoms of increasing size to ensure a constant concentration. Curves for different concentrations c are shown. Solid symbols correspond to optimal rectangular features; open symbols correspond to perfect square-shaped features. (b) Elastic energy per B atom for a periodic array of features of size 40 with increasing distance or periodicity. (c) Elastic energy per B atom for different aspect ratios for features in the size range of 40–55 and $c = 0$. Note that $c = 0$ is not truly a concentration 0 but a sufficiently small concentration to avoid feature-feature interactions.

A similar picture emerges for a larger system with 64 B atoms, and typical annealing results are shown in Figs. 1(d) and 1(e). Configuration (e) is slightly favored, by 0.055 eV. In both cases, we see a solid block of B atoms, and three more rows of B atoms at the bottom, which are separated by rows of A atoms. But it turns out that no annealing run has led to the configuration that is shown in Fig. 1(f), which we believe is the lowest-energy configuration for 64 B atoms. It is 0.061 eV lower in energy than configuration (e). This result was obtained by testing many configurations by hand; i.e., the results we have obtained from many annealing runs at different system sizes have guided us to manually perform energy calculations for configurations that are very similar. In general, we find that the lowest-energy configuration is not simply a solid block of B atoms, but a feature where the bottom row(s) of B atoms are separated from a more solid feature above. The number of these separated rows of B atoms increases, and our results indicate that $\sim 1/3$ of the rows tend to be separated.

The results presented in Fig. 1 are qualitatively the same for systems with different numbers of B atoms. In particular, we find that energetic considerations will always lead to a configuration with only one solid feature, rather than, for example, two (or several) equally sized solid features of half (or less) of its size. This can be seen in Fig. 2. In Fig. 2(b), we show the energy per B atom of a periodic arrangement of features of 40 B atoms as a function of the feature separation (which implies that the concentration c of B atoms decreases). The result is essentially the same for different feature sizes. The energy decreases as a function of separation, which means that two features want to be as far apart as possible. One is of course more interested in a constant alloy concentrations c. In Fig. 2(a) we therefore show the energy per particle of different feature sizes with different constants c. We first focus on the data for $c=1$ (solid circles), where we show results for N B atoms in periodic box of width N. The energy per B atom decreases monotonically as the number of B atoms in one feature increases, which implies that the largest possible (single) feature is favored. If we consider, for example, 160 B atoms that can be arranged either as one feature (of size 160) or four features (of size 40), we see that one big feature is favored by approximately 0.76 eV, which is significantly larger than k_BT.

The curves in Fig. 2(a) are not completely smooth, and certain sizes are preferred. As a general trend, we found that the lowest-energy configuration is typically obtained by forming a rectangular feature that is solid at the top with a few more rows that are detached (as discussed above) and that a feature with full rows and columns is preferred. For $c=0$, an aspect ratio of around 1.6 is preferred, as can be seen in Fig. 2(c), where we plot aspect ratios, rather than sizes, for all the data in the size range of 40–55. Our results suggest that the optimal aspect ratio becomes more square-like as c increases (data not shown). We also show data for perfect squares in Fig. 2(a) to illustrate that the decreasing energy is not an artifact of varying aspect ratios. The preference of one single feature becomes more (less) pronounced when c increases (decreases) and vanishes completely when $c=0$ (cf. curves for $c=2$ and $c=0$).

All the results discussed so far are for $r=2$ (i.e., nearest-neighbor bonds are slightly more important than diagonal bonds). But when r changes significantly, we obtain qualitatively very different results. For $r=20$ [cf. Fig. 3(a)], the nearest-neighbor terms dominate over diagonal bonds, and the B atoms arrange themselves into an essentially square-shaped checkerboard feature at the top of the A matrix, with a solid core of B atoms near the surface. In such an arrangement, most diagonal bonds have essentially the same length. In particular, diagonal A-A bonds and diagonal B-B bonds have the same length. This does not lead to a significantly higher energy because the contributions of these bonds are neglected. A system where the nearest-neighbor bonds dominate leads to a checkerboard pattern for the following reason: in a perfect checkerboard region, all the nearest-neighbor bonds are between A and B atoms. If we make the simplifying assumption that the checkerboard region is compressed to the lattice constant of the A matrix, then all bonds are compressed by 2%. But this is energetically preferred over half of the atoms (the B atoms) being compressed by 4%, as it would be the case in a solid feature. We note in passing that many empirical potentials have a cutoff between first and second nearest neighbors, which implies that $r=\infty$.

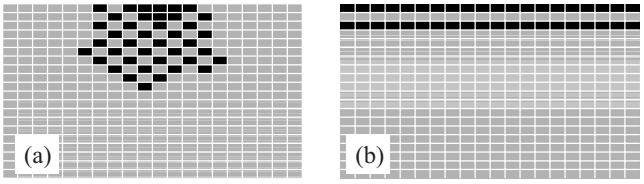

FIG. 3. Typical annealing results for 40 B atoms (black) in an array of 20×20 A atoms (gray) for the extreme cases of the bond ratio $r=20$ (a) and $r=0.05$ (b). We note that the same configurations with $r=2$ yield energies of 3.2 eV [cf. (a)] and 11.6 eV [cf. (b)], which is significantly higher than the energy for the configurations shown in Figs. 1(a)–1(c).

On the other hand, we get a rather different result when $r=0.05$ [Fig. 3(b)]. Here, the competition between the diagonal and nearest-neighbor bonds is dominated by the diagonal bonds. They can best assume (almost) their equilibrium length in a configuration that consists of horizontal stripes of B atoms. All columns now are the same, and they can relax upward. More precisely, the diagonal bonds assume almost their equilibrium length (and approach it in the limit that k_{diag} gets large), while the upward nearest-neighbor bonds are only slightly longer than their equilibrium length. It is essentially only the horizontal nearest-neighbor bonds between B atoms that contribute to the overall elastic energy, but this energy is small, compared to the contribution of the diagonal bonds, when k_{diag} is large. We note that the same configuration with the lower B stripe even lower has the same energy. We also note that this balance between nearest-neighbor bonds and diagonal bonds is ultimately the reason for the stripes of A atoms in the solid feature, as shown in Fig. 1.

We believe that for most systems it is plausible that effective nearest-neighbor bonds are more important than next-nearest-neighbor bonds, and that r is typically slightly larger than 1. Therefore, the results discussed above in Figs. 1, 2, and 3(a) are a rather general result. In particular, our results predict that there is lateral segregation in heteroepitaxial sys-

tems and that purely thermodynamic arguments lead to one large subsurface structure of the epilayer material. When the contributions of the diagonal bonds are very small, the atomistic details of the subsurface feature might change [cf. Fig. 3(a)], but we still find lateral segregation.

Our results are entirely based on equilibrium arguments. They do not predict a length scale in the system. However, under typical growth condition, the mobility of the epilayer type B atoms will be restricted. We therefore believe that in a real system, there will be a typical feature separation that is determined by the mobility of B atoms. Also, the inclusion of interface energies might result into a typical feature separation. Therefore, we expect several subsurface features, with a spacing that is dictated by the kinetics of the problem and interface energies. But as long as there is some mobility for the B atoms, the B atoms will not be distributed homogeneously; rather, there will be several subsurface features, similar to the ones shown in Fig. 1.

The work of Cullis and co-workers[5,6] suggests that vertical segregation is the driving force for island nucleation after a film of a certain thickness has been deposited. In other words, the onset of islanding might be controlled if one can manipulate the vertical segregation in the film. Our results suggest that, in addition, there is lateral segregation. The position of the subsurface features will undoubtedly be correlated with the position of the island formation since the effective misfit has been shown to influence island nucleation.[17–19] It is shown in Fig. 4 that the effective lattice constant is significantly larger above the subsurface features than it is above the areas in between. But variations in the relative lattice constant lead to variations in the mobility and chemical potential of atoms on the surface, and thus to variations in the nucleation probability.[17–19] Therefore, if one can control the separation of the subsurface features, one might have an additional parameter to control the positioning and spacing of quantum dots.

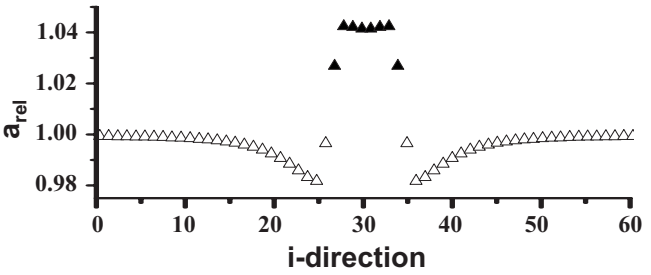

FIG. 4. Relative lattice constant above a subsurface feature of type B atoms as shown in Fig. 1. Solid (open) symbols denote positions above the (a) B atoms. The feature is embedded in a system of size 60 to illustrate the asymptotic approach of the lattice constant to the value 1.0. Lattice constants of 1.0 and 1.04 correspond to completely relaxed A and B atoms, respectively. The relative lattice constant at each site is defined as the average of the distances to the left and right; this definition explains the values right at the boundaries.

This research was supported in part by the MARCO Center on Functional Engineered NanoArchitectonics (FENA) and by the NSF through Grants No. DMS-0402276 and No. DMS-0439872-013151000.

[1] J. Eaglesham and M. Cerullo, Phys. Rev. Lett. **64**, 1943 (1990).
[2] Y. W. Mo, D. E. Savage, B. S. Swartzentruber, and M. G. Lagally, Phys. Rev. Lett. **65**, 1020 (1990).
[3] P. M. Petroff and S. B. Denbaars, Superlattices Microstruct. **15**, 15 (1994).
[4] J. A. Floro, E. Chason, R. D. Twesten, R. Q. Hwang, and L. B. Freund, Phys. Rev. Lett. **79**, 3946 (1997).
[5] A. G. Cullis, D. J. Norris, T. Walther, M. A. Migliorato, and M. Hopkinson, Phys. Rev. B **66**, 081305(R) (2002).
[6] M. A. Migliorato, A. G. Cullis, M. Fearn, and J. H. Jefferson, Phys. Rev. B **65**, 115316 (2002).
[7] Y. Tu and J. Tersoff, Phys. Rev. Lett. **93**, 216101 (2004).
[8] C. Priester and G. Grenet, Phys. Rev. B **61**, 16029 (2000).
[9] Z. F. Huang and R. C. Desai, Phys. Rev. B **65**, 195421 (2002).
[10] X. Z. Liao, J. Zou, D. J. H. Cockayne, J. Qin, Z. M. Jiang, X. Wang, and R. Leon, Phys. Rev. B **60**, 15605 (1999).
[11] T. Walther, A. G. Cullis, D. J. Norris, and M. Hopkinson, Phys. Rev. Lett. **86**, 2381 (2001).
[12] U. Denker, M. Stoffel, and O. G. Schmidt, Phys. Rev. Lett. **90**, 196102 (2003).
[13] G. Hadjisavvas and P. C. Kelires, Phys. Rev. B **72**, 075334 (2005).
[14] C. Lang, D. J. H. Cockayne, and D. Nguyen-Manh, Phys. Rev. B **72**, 155328 (2005).
[15] R. E. Caflisch, Y.-J. Lee, S. Shu, Y. Xiao, and J. Xu, J. Comput. Phys. **219**, 697 (2006).
[16] C. Connell, R. E. Caflisch, E. Luo, and G. Simms, J. Comput. Appl. Math. **196**, 368 (2006).
[17] B. Yang, F. Liu, and M. G. Lagally, Phys. Rev. Lett. **92**, 025502 (2004).
[18] X. Niu, R. Vardavas, R. E. Caflisch, and C. Ratsch, Phys. Rev. B **74**, 193403 (2006).
[19] X. B. Niu, Y. J. Lee, R. E. Caflisch, and C. Ratsch, Phys. Rev. Lett. **101**, 086103 (2008).